

LANGEVIN DYNAMICS IN 4-DIMENSIONAL MODEL OF NUCLEUS–NUCLEUS COLLISIONS *

J. BŁOCKI, O. MAZONKA, J. WILCZYŃSKI

Institute for Nuclear Studies
05-400 Otwock-Świerk, Poland

Z. SOSIN AND A. WIELOCH

Institute of Physics, Jagellonian University
Reymonta 4, 30-059 Kraków, Poland

(Received April 10, 2000)

Description of a realistic dynamic model of nucleus–nucleus collisions and fusion reactions, combined with stochastic effects (fluctuations) is given. We solve Langevin equations of motion in which stochastic white noise term is added to deterministic conservative and dissipative forces. The equations of motion are solved in 4-dimensional configuration space including three geometrical variables defining shape of the system and one variable defining charge asymmetry. Dissipative forces are calculated assuming one-body dissipation mechanism. Two sources of fluctuations are considered: thermal fluctuations determined by the fluctuation–dissipation theorem (Einstein relation) and fluctuations associated with exchange of nucleons. The width of the thermal fluctuations turns out to dominate stochastic effects in fusion reactions. It is shown that in near-threshold fusion reactions, the fluctuations remove flux from reseparation processes and direct it to fusion (and vice versa). Consequently, fluctuations enhance sub-barrier fusion reactions and lower the effective fusion threshold.

PACS numbers: 25.70.–z, 25.70.Jj, 24.60.Ky

1. Introduction

Recent synthesis of superheavy nuclei of the element $Z = 118$ [1] has intensified theoretical studies aimed to understand the mechanism of fusing of very heavy systems and to explain the role of fluctuations which probably decisively enhance fusion at the lowest near-threshold energies.

* Presented at the Kazimierz Grotowski 70th Birthday Symposium “Phases of Nuclear Matter”, Kraków, Poland, January 27–28, 2000.

In this paper we give description of our 4-dimensional semiclassical model of nucleus–nucleus collisions which had been developed and improved over several years and recently combined with a description of statistical fluctuations. Following works of Jarzynski [2] and earlier studies of Feldmeier [3], we have incorporated the statistical fluctuations to our classical model of nucleus–nucleus collisions in terms of the Langevin dynamics (see also Refs. [4, 5] and references therein).

2. Lagrange–Rayleigh equations of motion

Various classical models of nucleus–nucleus collisions are characterized by three basic ingredients, namely:

- (a) the collective degrees of freedom (q_i) which are treated explicitly, and their associated inertial parameters (momenta);
- (b) the potential energy $V(q_i)$;
- (c) the assumed dissipative forces (friction) which remove the energy from the collective degrees of freedom.

Having defined these basic ingredients one can compute the time evolution of the collective variables by solving the generalized Lagrange equations:

$$\frac{d}{dt} \frac{\partial \mathcal{L}}{\partial \dot{q}_i} - \frac{\partial \mathcal{L}}{\partial q_i} = - \frac{\partial \mathcal{F}}{\partial \dot{q}_i}. \quad (1)$$

Here $\mathcal{L}(q_i, \dot{q}_i) = T(q_i, \dot{q}_i) - V(q_i)$ is the Lagrangian of the system, and

$$\mathcal{F}(q_i, \dot{q}_i) = - \frac{1}{2} \frac{d}{dt} \{T(q_i, \dot{q}_i) + V(q_i)\}$$

is the Rayleigh dissipation function. In practice, for solving the coupled differential equations (1) it is necessary to retain only the minimum number of degrees of freedom q_i which are absolutely essential.

3. Shape parameterization

We use in our model the shape parametrization which has been proposed in Ref [6]. The axially symmetric shapes of fixed volume consist of two generally unequal spheres modified by a smoothly fitted portion of a third quadratic surface of revolution. A set of dimensionless degrees of freedom specifying the configuration are the following (see Fig. 1):

- 1) the distance variable, $\rho = r/(R_1 + R_2)$,
- 2) the neck variable, $\lambda = (l_1 + l_2)/(R_1 + R_2)$,
- 3) the asymmetry variable, $\Delta = (R_1 - R_2)/(R_1 + R_2)$. (2)

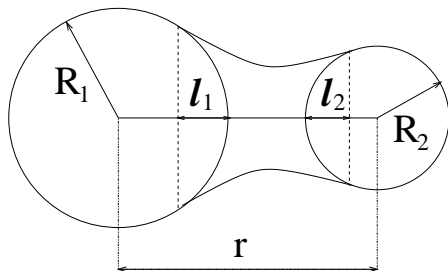


Fig. 1. Shape parameterization of the evolving composite system (pre-scission shape).

In the above, r is the distance between the centers of the spheres, whose radii are R_1 and R_2 . The quantities l_1, l_2 are the distances from the inner tips of the two spheres to the respective junction points with the middle quadratic surface of revolution. The natural boundaries of the configurational space (ρ, λ, Δ) were discussed in Ref. [6]. They are given by:

$$\rho \geq |\Delta|, \quad -1 \leq \Delta \leq 1, \quad 2 - (1 + \rho^{-1})|\Delta| \geq \lambda \geq \max\{0, 1 - \rho\}. \quad (3)$$

As it can be readily verified and seen from Fig. 2, the upper boundary for λ corresponds to egg-like shapes for which the middle quadratic has just covered up completely the smaller sphere. At the lower boundary we have separated spheres for $\lambda = 0$ and portions of intersecting spheres (without any middle quadratic surface) for $\lambda = 1 - \rho$. At scission the center quadratic degenerates into a cone, which implies $\lambda_{sc} = 1 - \rho_{sc}^{-1}$.

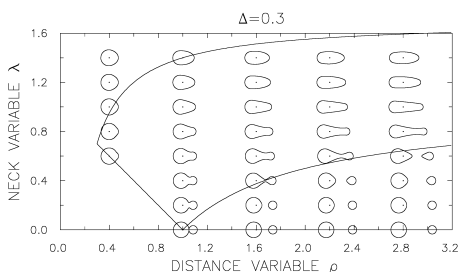


Fig. 2. A map of different shapes in (ρ, λ) -space for a fixed value of $\Delta = 0.3$. The straight line, $\rho + \lambda = 1$, corresponds to two intersecting spheres. There are no defined shapes under that line. Scission occurs when the $\lambda = 1 - \rho^{-1}$ line is crossed. Configurations below the scission line are two separated fragments. The upper boundary line, $\lambda = 2 - |\Delta|(1 + \rho^{-1})$, corresponds to the situation when smaller of the spheres is enclosed by the neck.

We have extended our model by introducing additionally the charge asymmetry variable

$$\Delta_Z = \frac{Z_1^{1/3} - Z_2^{1/3}}{Z_1^{1/3} + Z_2^{1/3}}. \quad (4)$$

It was found that this new degree of freedom, independent on the mass asymmetry Δ , plays an important role in early stage of nucleus–nucleus collisions, during equilibration of the N/Z ratio.

In addition to the macroscopic variables (ρ , λ , Δ , Δ_Z) there are three rotational degrees of freedom ($\theta_1, \theta_2, \theta_{\text{rel}}$) and three angular velocities ($\omega_1, \omega_2, \omega_{\text{rel}}$) connected with the rotation of sphere 1 and sphere 2 and the rotation of the shape as a whole.

As a parameter which controls the transition from separate nuclei to compound nucleus, we introduce the window opening parameter α (see Fig. 3):

$$\alpha = \frac{\sin \theta}{\sin \theta_{\text{max}}}. \quad (5)$$

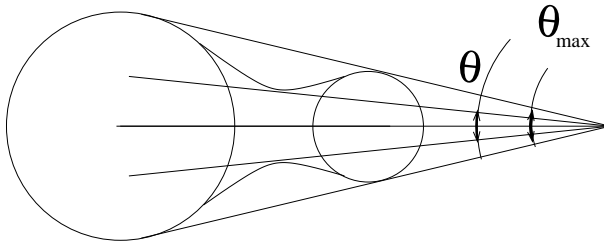


Fig. 3. Illustration of the window opening parameter, $\alpha = \sin \theta / \sin \theta_{\text{max}}$

4. Kinetic energy

For the kinetic energy we take a quadratic form in velocities with a mass tensor calculated in the Werner–Wheeler approximation [7]. It has been found that in the dynamical trajectory calculations the motion in the Δ direction was invariably overdamped to such an extent that the component of the inertia tensor M_{ij} associated with Δ could be safely neglected. The kinetic energy is then reduced to the form

$$T = \frac{1}{2} M_{\rho\rho} \dot{\rho}^2 + M_{\rho\lambda} \dot{\rho} \dot{\lambda} + \frac{1}{2} M_{\lambda\lambda} \dot{\lambda}^2. \quad (6)$$

The matrix element $M_{\rho\rho}$ of the mass tensor for two separated spheres is exactly the reduced mass.

In the rotational degrees of freedom the kinetic energy is equal to:

$$T_r = \frac{1}{2}(I_{\text{rel}}\omega_{\text{rel}}^2 + I_1\omega_1^2 + I_2\omega_2^2), \tag{7}$$

where I_1 and I_2 are the rigid moments of inertia of sphere 1 and 2, respectively and $I_{\text{rel}} = I_{\text{tot}} - I_1 - I_2$ where I_{tot} is the rigid moment of inertia of the whole system. Two spheres can rotate independently from the relative rotation, but due to the tangential friction, after some time all the frequencies ω_{rel} , ω_1 and ω_2 become equal and the system rotates as a rigid body (“sticking” limit).

The mass tensor is calculated from the density distribution (which is assumed to be uniform within the shape boundaries) and the collective velocity field. As shown by Feldmeier [3]), the mass tensor equals to:

$$M_{\varrho\varsigma} = \rho_d\pi \int \left(\frac{1}{2}B_\varrho B_\varsigma + P^2 A_\varrho A_\varsigma \right) dz \quad \varrho, \varsigma = \rho, \lambda, \Delta, \tag{8}$$

where $P = \bar{\rho}$ is the equation of the nuclear surface in cylindrical coordinates $(\bar{\rho}, z, \phi)$, and

$$A_\varrho = -\frac{1}{P^2} \int^z \frac{\partial P^2}{\partial \varrho} dz' - \frac{\pi}{V_0} \int \frac{\partial P^2}{\partial \varrho} z'' dz'', \tag{9}$$

$$B_\varrho = -\frac{1}{2} \frac{1}{P^2} \frac{\partial P^2}{\partial z} \int^z \frac{\partial P^2}{\partial \varrho} dz' + \frac{\partial P^2}{\partial \varrho}, \tag{10}$$

where V_0 is the total volume of the system

$$V_0 = \pi \int P^2 dz. \tag{11}$$

Moments of inertia are given by

$$I_{\text{tot}} = I_{\text{rel}} + I_1 + I_2, \tag{12}$$

$$I_{\text{tot}} = \rho_d\pi \int \left(\frac{1}{2}P^4 + P^2 z^2 \right) dz - \frac{\rho_d\pi^2}{V_0} \left(\int P^2 z dz \right)^2, \tag{13}$$

$$I_{1,2} = \rho_d \frac{4\pi}{15} R_{1,2}^5. \tag{14}$$

5. Potential energy

The potential energy of a nuclear system is calculated for a given shape as the sum of the nuclear potential energy and the Coulomb energy. The nuclear part is calculated by the double folding procedure developed by Krappe, Nix and Sierk [8]:

$$V_n = -\frac{C_s}{8\pi^2 r_0^2 a^3} \iint \left(\frac{1}{a} - \frac{2}{\sigma} \right) \exp(-\sigma/a) d^3\mathbf{r} d^3\mathbf{r}', \quad (15)$$

where $\sigma = |\mathbf{r} - \mathbf{r}'|$, $C_s = a_s(1 - k_s I^2)$ and $I = (N - Z)/A$. The parameters r_0 , a , a_s and k_s are taken from the fit done in Ref. [8]. For axially symmetric shapes formula (15) reduces to the three dimensional integral of the following type:

$$V_n = \frac{C_s}{4\pi r_0^2} \iiint \left(2 - \left[\left(\frac{\sigma}{a} \right)^2 + 2\frac{\sigma}{a} + 2 \right] \exp -\frac{\sigma}{a} \right) \times \frac{P_2(z, z')P_2(z', z)}{\sigma^4} dz dz' d\phi, \quad (16)$$

where

$$P_2(z, z') = P(z) \left(P(z) - P(z') \cos \phi - \frac{dP}{dz}(z - z') \right), \\ \sigma^2 = P(z)^2 + P(z')^2 - 2P(z)P(z') \cos \phi + (z - z')^2.$$

A similar procedure has to be done in calculating the Coulomb part of the potential which for an axially symmetric shape can be written as:

$$V_c = \frac{\pi}{3} \rho_z \rho_{z'} \iiint \frac{P_2(z, z')P_2(z', z)}{\sigma} dz dz' d\phi, \quad (17)$$

where ρ_z and $\rho_{z'}$ are the charge densities.

6. Shell effects

The importance of shell effects in fusion reactions was demonstrated experimentally as an enhanced fusion probability in reactions involving magic or near-magic nuclei, such as ^{208}Pb or ^{209}Bi . Shell effects are included in our calculations in a phenomenological form proposed by Myers and Swiatecki [9, 10]. In this simple approach the shell correction $S_0(N, Z)$ to the potential energy is written in the form

$$S_0(N, Z) = (5.8 \text{ MeV}) \left(\frac{F_N + F_Z}{\frac{A^{2/3}}{2}} - 0.325A^{1/3} \right), \quad (18)$$

where

$$F_N = q_N(N - N_{i-1}) - \frac{3}{5} \left(N^{5/3} - N_{i-1}^{5/3} \right)$$

with

$$q_N = \frac{3}{5} \frac{N_i^{5/3} - N_{i-1}^{5/3}}{N_i - N_{i-1}}.$$

Here N_{i-1} and N_i are the closed shell neutron numbers adjacent to the actual number of neutrons N of a given nucleus of mass number A . Identical formulae for F_Z and q_Z describe the shell effect for protons. According to this prescription, for the double closed shell nucleus ^{208}Pb the shell effect is $S_0 = -11.2$ MeV.

The shell correction $S_0(N, Z)$ defined above refers to spherical shapes. For deformed shapes the shell correction is attenuated as suggested in Refs. [9, 10]:

$$S(N, Z) = S_0(N, Z) \left(1 - 2 \frac{\text{dist}^2}{a^2} \right) \exp \left(- \frac{\text{dist}^2}{a^2} \right), \quad (19)$$

where dist^2 is a measure of deviation from spherical shape,

$$\text{dist}^2 = \int \frac{d\Omega}{4\pi} (r(\theta, \phi) - R_0)^2.$$

Here $r(\theta, \phi)$ is the radius vector describing the given shape and R_0 is the radius of the equivalent sphere.

Considering shape evolution of nuclear systems, it is necessary to interpolate in a smooth way between the sum of the shell corrections S_1 and S_2 of the colliding nuclei in the entrance channel and the shell correction S_c of the mononuclear shape. We adopted an interpolation in terms of the degree of communication between the two nuclei as specified by the ‘‘window opening’’ parameter α defined by Eq. (5):

$$S = (1 - \alpha)(S_1 + S_2) + \alpha S_c. \quad (20)$$

For separated shapes (below the scission line) $\alpha = 0$ and thus $S = S_1 + S_2$. When the neck loses its concavity at $\alpha = 1$ the shell correction becomes a pure mononucleus shell correction S_c . This is kept for all convex shapes with $\alpha > 1$.

It should be noted here that we do not consider thermal attenuation of the shell corrections. This can be justified as long as our model is restricted for a description of near-threshold fusion reactions at low excitation energies.

7. Dissipation

In our model, we restrict ourselves to one-body dissipation [11], arising from collisions of independent particles with the moving boundary of the nucleus. In the one-body dissipation model [11], the energy flow from collective to intrinsic motion is attributed to the interaction of individual nucleons with the mean field produced by all nucleons in the system. In a simplified picture this interaction may be viewed as mediated by collisions between nucleons and a moving container wall, or by the passage of nucleons from one fragment to the other through a window.

There are two limiting cases in which two different simple formulae for the rate of the dissipated energy can be derived. The first one is so called the mononuclear regime when the system of colliding ions can be considered as a monosystem with a thick neck. In that case the gas of nucleons can be considered as a relaxed Fermi gas and the rate of the energy dissipation is given by the following wall formula [11]:

$$\dot{E}_{\text{wall}} = \rho \bar{v} \oint dS (\dot{n} - v_d)^2, \quad (21)$$

where ρ is the mass density of nucleons, \bar{v} is their average speed (equal to three quarters of the Fermi velocity in the Fermi gas model), dS is an element of nuclear surface, \dot{n} is the normal velocity of walls and v_d is the overall drift velocity of the gas of nucleons ensuring the invariance of Eq. (21) against translations and rotations.

In the second limiting case, the dinuclear regime, when two ions are either separated or connected by a thin neck, Eq. (21) cannot be applied as we are dealing with two Fermi gases separated by the collective velocity. In that case the so-called “wall-plus-window” formula can be applied and it reads as follows:

$$\dot{E}_{\text{w+w}} = \rho \bar{v} \int_1 dS (\dot{n} - v_{d1})^2 + \rho \bar{v} \int_2 dS (\dot{n} - v_{d2})^2 + \frac{1}{4} \rho \bar{v} \sigma (u_t^2 + 2u_r^2) + \frac{16}{9} \frac{\rho \bar{v}}{\sigma} \dot{V}_1^2. \quad (22)$$

The first two terms represent the wall formula, Eq. (21), applied to each fragment separately, with drift velocities v_{d1} and v_{d2} , respectively. The third term is associated with the dissipation due to the exchange of particles through the window of the area σ , connecting the two nuclei moving with a relative velocity u . The components of the relative velocity, u_t and u_r , are parallel and perpendicular to the window, respectively. The last term in Eq. (22) corresponds to the dissipative resistance against the asymmetry changes [12,13] with \dot{V}_1 being the rate of the change of the volume of fragment 1. Eqs. (21) and (22) express the rate of the dissipated energy in two

limiting cases of the mononuclear and dinuclear regimes. In the intermediate configurations a smooth transition between formulae (21) and (22) is used [14]:

$$\dot{E} = f\dot{E}_{\text{wall}} + (1 - f)\dot{E}_{\text{w+w}} \quad (23)$$

with a formfactor f approaching a value $f = 1$ for sphere or spheroid-like shapes, and $f = 0$ at scission.

Following Feldmeier [3], we have introduced an additional dynamical equation, accounting for the coupling between the particle and entropy fluxes, which drives particles from hotter to colder gas. The time derivative of the difference of excitation energies of two parts of the nuclear system is given by:

$$\frac{d}{dt}(E_1^* - E_2^*) = \dot{E}_{1 \text{ wall}} - \dot{E}_{2 \text{ wall}} + 2T_0\dot{S}_{21}, \quad (24)$$

where the last term represents the effect of the temperature feedback which is proportional to the average temperature $T_0 = (T_1 + T_2)/2$ and the entropy flux \dot{S}_{21} taken from Ref. [3].

8. Langevin equation

Description of the nucleus–nucleus collisions in terms of the classical Lagrange–Rayleigh equations Eq. (1) with dissipative forces discussed in the previous section does not give satisfactory results, especially in attempts to explain fusion processes at low, near-threshold energies, when apparently the tails of fluctuating phenomena play very important role.

The dissipative dynamics basically stems from nonequilibrium statistical mechanics which relates two different macroscopic phenomena, fluctuations and dissipation, demonstrating their common microscopic origin. The connection between dissipation and macroscopic fluctuations follows from the microscopic description, under the condition the physical systems continuously evolves toward equilibrium. Thus having defined the dissipation mechanism, we can strictly determine the character of fluctuations. This is given by the Einstein relation (originally derived for Brownian motion),

$$\gamma = \frac{D}{2T}, \quad (25)$$

which relates the friction coefficient γ and the momentum diffusion coefficient D at the temperature T . This relation follows from the general fluctuation–dissipation theorem, one of the most fundamental results of nonequilibrium statistical mechanics.

From two alternative possibilities of implementation of fluctuations to the dynamical model, the Fokker–Planck and Langevin approaches, we have chosen the latter. The Fokker–Planck approach is appropriate for description of an ensemble of trajectories in the collective coordinate phase space, a type of analysis difficult to simulate numerically. On the contrary, the Langevin approach can be used in much easier numerical simulations of a single trajectory.

Denoting by Q the collective degrees of freedom, by P their associated momenta and by M the corresponding inertia parameters, the Langevin equations of motion for a trajectory look as follows:

$$\frac{dQ}{dt} = \frac{P}{M}, \quad \frac{dP}{dt} = -\frac{dV}{dQ} + F_{\text{fric}} + \tilde{F}_{\text{fluc}}, \quad (26)$$

where

$$F_{\text{fric}} = -\gamma\dot{Q}, \quad (27)$$

is an average friction force resulting from the coupling to the nucleonic “heat bath”, whereas \tilde{F}_{fluc} is a rapidly fluctuating stochastic force determining fluctuations in momentum according to the value of the coefficient $D(Q, P)$ given by Eq. (25). The force \tilde{F}_{fluc} can be simulated numerically by repeatedly producing a random kick δP in the collective momentum. The value of δP is chosen randomly from a Gaussian distribution, with a mean value and variance given by:

$$\overline{\delta P} = 0, \quad (28)$$

$$\overline{(\delta P)^2} = D \delta t, \quad (29)$$

where δt is a small time step between kicks.

9. Fluctuations

9.1. Thermal fluctuations

Equation (25) determines the magnitude of thermal fluctuations resulting from the coupling of the collective degrees of freedom to the nucleonic “heat bath”. Applying the Langevin approach to our macroscopic dynamic model with one-body dissipation we need to derive the momentum diffusion coefficient from the rate of energy dissipation in the “wall” and “window” mechanisms. For example, in case of the wall formula (21) the friction coefficient $\gamma = -F_{\text{fric}}/\dot{Q}$ (see Eq. (27)) can be expressed as

$$\gamma = \rho\bar{v} \oint dS \left(\frac{\partial n}{\partial Q} \right)^2 \quad (30)$$

because for a given surface element, \dot{n} can be written as $\dot{Q} \partial n / \partial Q$, where $(\partial n / \partial Q) dQ$ gives the normal outward displacement of the surface element accompanying an infinitesimal change dQ in the value of the collective coordinate.

Having determined the friction coefficient γ resulting from the one-body dissipation formula (22), the momentum diffusion coefficient D for thermal fluctuations is immediately obtained from the Einstein relation (25).

9.2. Exchange of particles

Apart from thermal fluctuations, also fluctuations in the number of exchanged nucleons contribute to the stochastic Langevin force. However this effect influences only the asymmetry degree of freedom. We assume that the motion of nucleons is chaotic and the correlation time is infinitesimally small. Then, for sufficiently short period of time, the exchange of nucleons can be treated as a Poisson process with the distribution undergoing the binomial law. Let us consider the number of particles passed from nucleus 1 to nucleus 2 during a time interval Δt to be N_1 and from 2 to 1 to be N_2 . Then the change of the atomic mass number of nucleus 1 is equal to:

$$\Delta A_1 = g = N_2 - N_1. \tag{31}$$

This quantity can be rewritten as a sum of average term and fluctuating term with zero mean value:

$$\Delta A_1 = \tilde{g} + \bar{g} + \Delta L, \quad \langle \Delta L \rangle = 0. \tag{32}$$

The diffusion coefficient D_A is defined by relation:

$$\langle \Delta L^2 \rangle = D_A \Delta t = \langle \tilde{g}^2 \rangle - \bar{g}^2. \tag{33}$$

Since quantities N_1 and N_2 are independent and are taken from binomial distributions, the following equivalencies:

$$\langle N_1 N_2 \rangle = \langle N_1 \rangle \langle N_2 \rangle \quad \text{and} \quad \langle N_i^2 \rangle = \langle N_i \rangle^2 + \langle N_i \rangle \left(1 - \frac{\langle N_i \rangle}{A_i} \right) \tag{34}$$

lead to the explicit expression for $\langle \Delta L^2 \rangle$:

$$\langle \Delta L^2 \rangle = \langle N_1 \rangle + \langle N_2 \rangle - \left(\frac{\langle N_1 \rangle^2}{A_1} + \frac{\langle N_2 \rangle^2}{A_2} \right). \tag{35}$$

We denote A_1 and A_2 atomic mass numbers and $A = A_1 + A_2$. As it follows from the “window” formula (see the third term in Eq. (22)), the average number of particles exchanged through the window of the area σ is:

$$\langle N_1 \rangle \approx \langle N_2 \rangle \approx \frac{1}{4} \sigma \bar{v} n \Delta t, \tag{36}$$

where \bar{v} is the average velocity and n is the concentration of nucleons (number per unit volume). Hence we obtain the expression for D_A :

$$D_A = \frac{1}{2}\sigma\bar{v}n - \frac{1}{16\mathcal{A}}\sigma^2\bar{v}^2n^2\Delta t, \quad (37)$$

where $\mathcal{A} = A_1A_2/(A_1 + A_2)$. The limit when two containers can be treated as infinite reservoirs of particles is achieved when the time interval Δt is small enough:

$$\Delta t \ll \frac{8a}{\sigma\bar{v}n}. \quad (38)$$

Transforming the obtained result to fluctuations in the asymmetry variable Δ we use the following relations:

$$\dot{\Delta} = f\dot{A}_1, \quad D_\Delta = f^2D_A, \quad (39)$$

where

$$f = \left. \frac{\partial\Delta}{\partial A_1} \right|_A = \frac{2}{3} \frac{(A_1 + A_2)A_1^{-2/3}A_2^{-2/3}}{(A_1^{1/3} + A_2^{1/3})^2}. \quad (40)$$

10. Parameterization of the potential

Numerical simulations of stochastic fusion processes in our 4-dimensional model are very time consuming, mostly because the potential energy cannot be expressed analytically and must be calculated as three-dimensional integral (Eqs. (16) and (17)) at each point along the Langevin trajectory. Each trajectory consists of hundreds of points and at each point one has to calculate conservative forces in four directions: $(\rho, \lambda, \Delta, \Delta_Z)$. It is clear that calculation of millions of trajectories, necessary for simulation of the Langevin dynamics, becomes in practice impossible.

Here we propose a method which can speed up the calculations. Similarly to Ref. [15], we parameterize the potential in order to avoid calculation of three-dimensional integral at each point. The simplest way is to create four-dimensional lattice in the phase space and map the potential. Then, having values of the potential on the lattice, one can determine a value of the potential in any intermediate point by interpolation.

Simple estimation shows that a lattice of size 100^4 takes about 200 Mb of the computer memory and, of course, a long CPU time to calculate the potential. However, we can use the property that the potential energy is symmetric with respect to the transformation $(\Delta, \Delta_Z) \rightarrow (-\Delta, -\Delta_Z)$. Moreover, it can be noted that the parameter Δ_Z is strongly related to Δ : the potential rises fast on the way from its minimum in the direction $(\Delta = 1, \Delta_Z = -1)$, while it rises much slower in the direction $(\Delta = 1, \Delta_Z = 1)$.

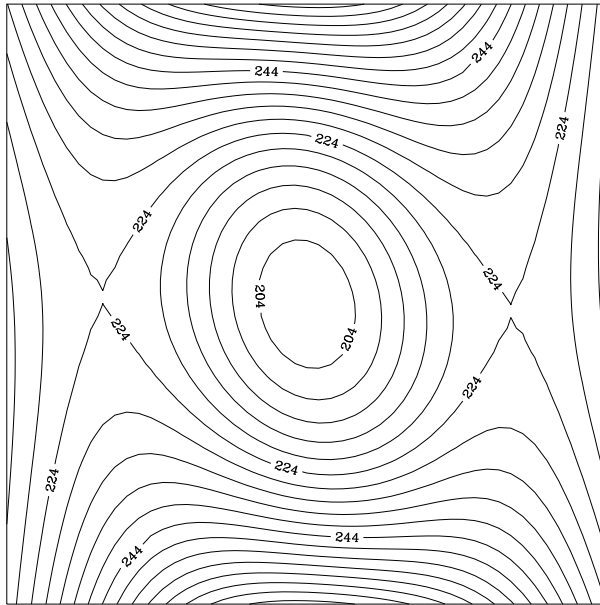


Fig. 4. The potential energy in the (Δ, Δ'_Z) -subspace, $\Delta = (-0.5, 0.5)$ vs $\Delta'_Z = (-0.05, 0.05)$, for the system $^{86}\text{Kr}+^{136}\text{Xe}$ at the point $\rho = 1.26$, $\lambda = 0.05$, which corresponds to the beginning of the trajectory near touching configuration. Shell corrections are not included. Contour lines correspond to levels of the potential energy in MeV with respect to the potential energy of separated nuclei.

Therefore one can replace the parameters (Δ, Δ_Z) with (Δ, Δ'_Z) , where $\Delta'_Z = \Delta_Z - \Delta$, saving the inversion symmetry as for the original pair of parameters. Disregarding shell effects, the potential around the point $(\Delta = 0, \Delta'_Z = 0)$ has a regular well-shape in coordinates $x = \Delta$ and $y = \Delta'_Z$ (see Fig. 4). Therefore we have chosen parameterization in that subspace as a 4-th degree polynomial:

$$z = f_1 + f_2x^2 + f_3xy + f_4y^2 + f_5x^4 + f_6x^3y + f_7x^2y^2 + f_8xy^3 + f_9y^4, \quad (41)$$

which represents the expansion of the potential z around $(0,0)$ -point. The symmetry property eliminates the odd degree terms.

The potential in the subspace (ρ, λ) is parameterized by a bilinear interpolation of the lattice points. Eq. (41) can be rewritten:

$$z = \vec{f} \cdot \vec{p}(x, y), \quad (42)$$

where

$$\vec{p}(x, y) = (1, x^2, xy, y^2, x^4, x^3y, x^2y^2, xy^3, y^4)$$

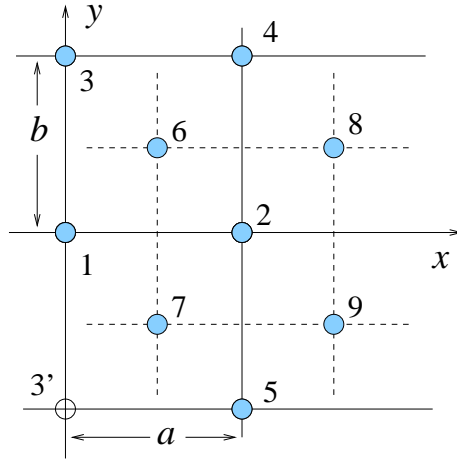


Fig. 5. Choice of points for determination of the coefficients in polynomial expansion of the potential around (0,0)-point in the (Δ, Δ_Z) -subspace. Point 1 is the origin of the coordinate system.

and $\vec{f} = (f_1, f_2, f_3, f_5, f_6, f_7, f_8, f_9)$. Now let us choose 9 points as shown on Fig. 5 giving the values $\vec{z} = (z_1, z_2, z_3, z_5, z_6, z_7, z_8, z_9)$. Then the coefficients \vec{f} can be found from the equation:

$$\hat{M} \cdot \vec{f} = \vec{z}, \tag{43}$$

where

$$\hat{M} = \begin{pmatrix} \vec{p}(0, 0) \\ \vec{p}(a, 0) \\ \vec{p}(0, b) \\ \vec{p}(a, b) \\ \vec{p}(a, -b) \\ \vec{p}(\frac{a}{2}, \frac{b}{2}) \\ \vec{p}(\frac{a}{2}, -\frac{b}{2}) \\ \vec{p}(\frac{3a}{2}, \frac{b}{2}) \\ \vec{p}(\frac{3a}{2}, -\frac{b}{2}) \end{pmatrix} = \begin{pmatrix} 1 & 0 & 0 & 0 & 0 & 0 & 0 & 0 & 0 \\ 1 & a^2 & 0 & 0 & a^4 & 0 & 0 & 0 & 0 \\ 1 & 0 & 0 & b^2 & 0 & 0 & 0 & 0 & b^4 \\ 1 & a^2 & ab & b^2 & a^4 & a^3b & a^2b^2 & ab^3 & b^4 \\ 1 & a^2 & -ab & b^2 & a^4 & -a^3b & a^2b^2 & -ab^3 & b^4 \\ 1 & \frac{a^2}{4} & \frac{ab}{4} & \frac{b^2}{4} & \frac{a^4}{16} & \frac{a^3b}{16} & \frac{a^2b^2}{16} & \frac{ab^3}{16} & \frac{b^4}{16} \\ 1 & \frac{a^2}{4} & -\frac{ab}{4} & \frac{b^2}{4} & \frac{a^4}{16} & -\frac{a^3b}{16} & \frac{a^2b^2}{16} & -\frac{ab^3}{16} & \frac{b^4}{16} \\ 1 & \frac{9a^2}{4} & \frac{3ab}{4} & \frac{b^2}{4} & \frac{81a^4}{16} & \frac{27a^3b}{16} & \frac{9a^2b^2}{16} & \frac{3ab^3}{16} & \frac{b^4}{16} \\ 1 & \frac{9a^2}{4} & -\frac{3ab}{4} & \frac{b^2}{4} & \frac{81a^4}{16} & -\frac{27a^3b}{16} & \frac{9a^2b^2}{16} & -\frac{3ab^3}{16} & \frac{b^4}{16} \end{pmatrix}. \tag{44}$$

The exact solution for \vec{f} is the following:

$$\begin{aligned} f_1 &= z_1, \\ f_2 &= \frac{-18z_1 + 18z_2 - 2z_3 + z_4 + z_5 + 2z_6 + 2z_7 - 2z_8 - 2z_9}{12a^2}, \\ f_3 &= \frac{-z_4 + z_5 + 16z_6 - 16z_7}{6ab}, \end{aligned}$$

$$\begin{aligned}
f_4 &= \frac{-42z_1 - 18z_2 + 2z_3 - 3z_4 - 3z_5 + 30z_6 + 30z_7 + 2z_8 + 2z_9}{12b^2}, \\
f_5 &= \frac{6z_1 - 6z_2 + 2z_3 - z_4 - z_5 - 2z_6 - 2z_7 + 2z_8 + 2z_9}{12a^4}, \\
f_6 &= \frac{-3z_6 + 3z_7 + z_8 - z_9}{3a^3b}, \\
f_7 &= \frac{2z_1 - 2z_2 - 2z_3 + z_4 + z_5}{2a^2b^2}, \\
f_8 &= \frac{2z_4 - 2z_5 - 5z_6 + 5z_7 - z_8 + z_9}{3ab^3}, \\
f_9 &= \frac{30z_1 + 18z_2 + 10z_3 + 3z_4 + 3z_5 - 30z_6 - 30z_7 - 2z_8 - 2z_9}{12b^4}.
\end{aligned} \tag{45}$$

The procedure described above greatly speeds up the calculation especially when the parametrized potential is used for calculating ensembles of Langevin trajectories with high statistics.

11. Calculations

In this section we give some examples of calculations carried out with our model. Emphasis is put on interpretation of fusion reactions, especially at low, near-threshold energies at which fluctuations play a very important role and enhance the sub-barrier fusion cross sections by orders of magnitude.

Figure 6 shows an example of a contour map of the potential energy (with shell corrections included) in the reaction $^{86}\text{Kr}+^{70}\text{Ge}$, calculated in the subspace (ρ, λ) , for fixed value of the mass asymmetry Δ corresponding to the entrance channel asymmetry and charge asymmetry $\Delta_Z = 0$. There are two deterministic central-collision trajectories calculated for this system at energies near the fusion threshold. At $E_{\text{cm}} = 134$ MeV the colliding system approaches the touching configuration approximately at $(\rho = 1.3, \lambda = 0)$, then moves toward larger λ -values (a neck is developed) and finally slides down behind the saddle point $(\rho = 1.6, \lambda = 0.7)$ undergoing fusion. (For better understanding the sequence of shapes see also Fig. 3.) The second trajectory in Fig. 6 starts from the same point in the configurational space, but at slightly lower energy, $E_{\text{cm}} = 132$ MeV. This trajectory, however, is deflected outward and the system reseparates. Thus, the probability of fusion of the $^{86}\text{Kr}+^{70}\text{Ge}$ system, calculated in the classical deterministic approach, is $P_{\text{fus}} = 1$ at $E_{\text{cm}} = 134$ MeV and $P_{\text{fus}} = 0$ at $E_{\text{cm}} = 132$ MeV.

Fluctuations bring indeterminism to the reaction dynamics because for the same initial conditions, trajectories can either go to fusion or to reseparation. This is illustrated in Fig. 7 for the same reaction $^{86}\text{Kr}+^{70}\text{Ge}$ at

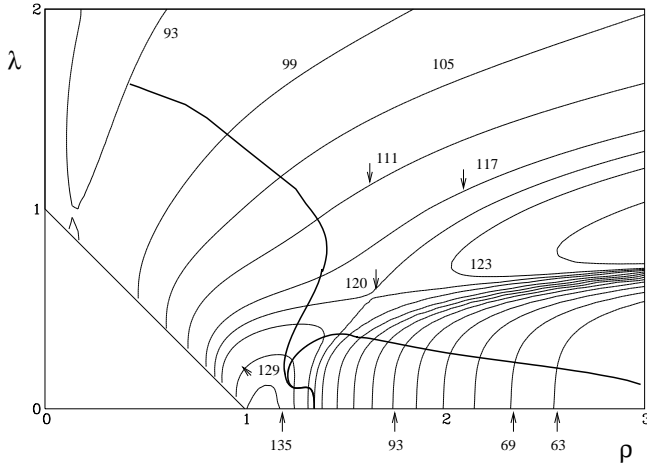


Fig. 6. Two deterministic trajectories for the $^{86}\text{Kr}+^{70}\text{Ge}$ colliding system, starting with initial kinetic energy 132 and 134 MeV and plotted on the potential energy map in (ρ, λ) -space. The energy contours are in MeV.

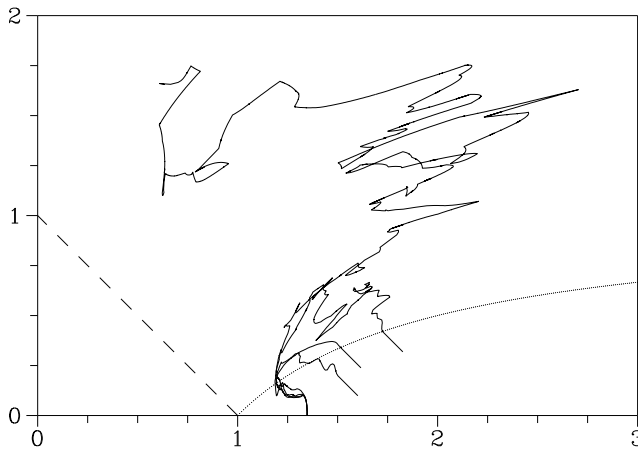


Fig. 7. Stochastic trajectories for the $^{86}\text{Kr}+^{70}\text{Ge}$ reaction. Four trajectories with included thermal fluctuations start with the same kinetic energy 132 MeV.

$E_{\text{cm}} = 132$ MeV for which deterministic calculation gives $P_{\text{fus}} = 0$. Calculations with thermal fluctuations included produce very irregular trajectories which show features of “random walk” under influence of the stochastic Langevin force. Out of four trajectories presented in Fig. 7, three lead to reparation of the colliding system, but one trajectory goes now to fusion, indicating that the fusion probability is in fact about $\frac{1}{4}$ and not zero, as in the deterministic calculation.

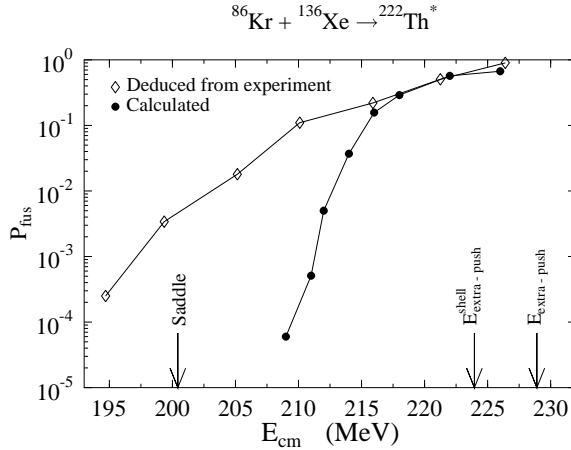


Fig. 8. Fusion probabilities extracted from measured compound–residue cross sections in the $^{86}\text{Kr}+^{136}\text{Xe}$ reaction [16], compared with the stochastic model calculations.

Having implemented the Langevin dynamics to our 4-dimensional configuration-space model we performed analysis of the near-threshold fusion probabilities for the $^{86}\text{Kr}+^{136}\text{Xe}$ reaction studied at GSI Darmstadt [16]. As the calculation are very time consuming, theoretical predictions of the fusion probabilities obviously are much easier than calculations of unrefined fusion cross sections requiring integration in l -space. Results of the comparison are presented in Fig. 8. It is seen that the fusion probabilities deduced from the measured compound–residue cross sections increase from $P_{\text{fus}} \approx 2 \times 10^{-4}$ at $E_{\text{cm}} = 195$ MeV to $P_{\text{fus}} \approx 1$ at $E_{\text{cm}} = 230$ MeV. Our calculations show that for energies $E_{\text{cm}} > 215$ MeV the calculated fusion probabilities agree with those deduced from experiment, despite the fact that the model in the deterministic version (without fluctuations) predicts the energy threshold for fusion ($P_{\text{fus}} = 0$) at a value indicated in Fig. 8 as $E_{\text{extra-push}}^{\text{shell}}$, *i.e.*, at $E_{\text{cm}} \approx 224$ MeV. However the enhancement of the calculated fusion probability caused by fluctuations is too small to reach agreement with the data. The calculated fusion threshold is moved down from $E_{\text{cm}} = 224$ MeV to about $E_{\text{cm}} = 210$ MeV, but the curve deduced from measured cross sections extends to still lower energies, even below $E_{\text{cm}} = 200$ MeV.

We admit that it is difficult to draw firm conclusions on the basis of the comparison presented in Fig. 8 because extraction of the “experimental” values of the fusion probability P_{fus} from the compound–residue cross sections is very model-dependent, especially for such heavy systems as $^{86}\text{Kr}+^{136}\text{Xe}$, for which fusion–fission reactions dominate, while details of the competition between neutron emission and fission are strongly influenced by not well known structural effects.

The above arguments led us to implementation of the method of parametrization of the potential energy (see Section 10) which made Langevin dynamics calculations of unrefined fusion cross sections feasible, especially while using additionally the importance sampling method in trajectory simulations characterized by low P_{fus} -values [17,18]. Calculations of fusion cross sections certainly take much more time than calculations of the fusion probability in central collisions because the former require inclusion of additional dimension, the angular momentum. The fusion cross section at the kinetic energy E can be calculated as a sum of contributions of partial waves:

$$\sigma_E = \pi \lambda^2 \sum (2l + 1) T_l, \quad (46)$$

where λ is the de Broglie wavelength, $\lambda^2 = \hbar^2/2\mu E_{\text{cm}}$, and T_l is the transmission coefficient for a given partial wave. In deterministic version of our dynamical model the transmission coefficient T_l is just a step function:

$$T_l = \begin{cases} 1 & \text{for } l \leq l_0, \\ 0 & \text{for } l > l_0, \end{cases} \quad (47)$$

where l_0 is the critical angular momentum for a given bombarding energy E , *i.e.*, the largest l -value for which deterministic trajectory still leads to fusion, while for all higher partial waves the system reseparates. Inclusion of fluctuations causes spreading of T_l -values as shown in Fig. 9: Step-function distributions are replaced by very diffused distributions extending to much larger l -values than respective critical angular momenta l_0 . For determination of the fusion cross sections it is necessary to calculate these T_l -distributions for each studied energy. Hundreds or even thousands Langevin trajectories have to be simulated at each (E, l) initial condition.

In order to investigate to what extent fluctuations can explain the enhancement of the fusion cross sections at near-barrier energies we selected the $^{86}\text{Kr} + ^{70}\text{Ge}$ reaction for which Reisdorf *et al.* [19] precisely measured the fusion excitation function in the whole sub-barrier region. The $^{86}\text{Kr} + ^{70}\text{Ge}$ system is only moderately heavy, so the measured compound-residue cross sections still well represent the total fusion cross sections, *i.e.*, contribution of the fusion-fission processes is small, at least at near threshold energies. Figure 10 displays results of our calculations for this system. The dashed line shows predictions of our model without fluctuations. In this deterministic approach, the fusion cross section has a sharp threshold at $E_{\text{cm}} \approx 133$ MeV, representing the height of the s -wave barrier increased by the dissipative loss of kinetic energy on the way to the barrier. As it is seen from Fig. 10, the deterministic fusion threshold is located about 10 MeV above the experimental threshold.

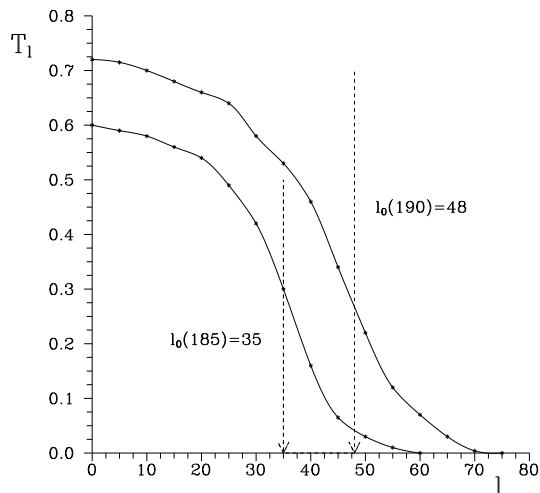


Fig. 9. Examples of “diffusion” of the transmission coefficients caused by thermal fluctuations. The transmission coefficients are calculated for the $^{86}\text{Kr}+^{104}\text{Ru}$ reaction at $E_{\text{cm}} = 190$ MeV (upper curve) and 185 MeV (lower curve). Limits of sharp cut-off distributions corresponding to deterministic calculation without fluctuations are indicated by arrows.

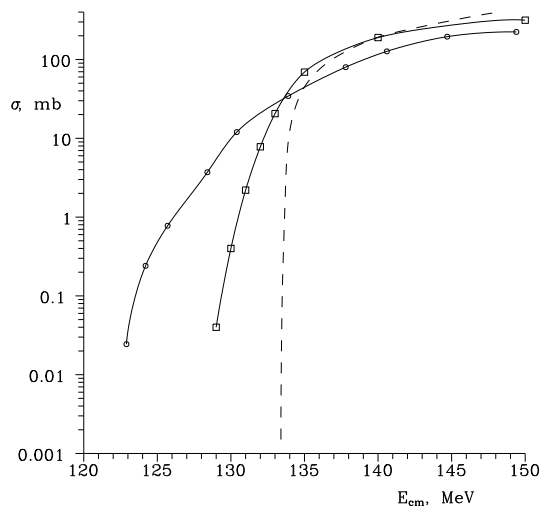


Fig. 10. Fusion excitation function for the $^{86}\text{Kr}+^{70}\text{Ge}$ reaction measured by Reisdorf *et al.* [19] (circles), compared with the stochastic model calculations (squares). The dashed line shows the excitation function obtained in deterministic limit without fluctuations.

Inclusion of fluctuations considerably enhances the fusion cross sections below the deterministic energy threshold, but the calculated excitation function moves only half-way toward the experimental curve. Our stochastic model calculations have been carried out assuming both thermal fluctuations and fluctuations associated with exchange of nucleons (see Section 9). The calculations have demonstrated that thermal fluctuations play decisive role, especially at near-threshold energies. Magnitude of the thermal fluctuations is determined by Einstein relation (25) and certainly cannot be treated as free parameter. Nevertheless, we performed calculations with larger values of the momentum diffusion coefficient and found that experimental fusion excitation function can be well reproduced assuming a value of D approximately two times larger than that resulting from Eq. (25). Of course such a large value of D has no physical justification.

We conclude that thermal fluctuations play a very important role in near-threshold and sub-barrier fusion reactions. The fluctuations remove flux from reseparation processes and direct it to fusion (and *vice versa*). Consequently, fluctuations enhance sub-barrier fusion reactions and lower the effective fusion threshold. However magnitude of thermal fluctuations determined by the Einstein relation is too small to obtain good quantitative agreement with experimental results.

This work was supported by the Polish–American Maria Skłodowska-Curie Joint Fund II, under Project No. PAA/DOE-98-34, and by the Polish–French project POLONIUM.

REFERENCES

- [1] V. Ninov *et al.*, *Phys. Rev. Lett.* **83**, 1104 (1999).
- [2] C. Jarzynski, *Phys. Rev.* **E56**, 5018 (1997); also private communication.
- [3] H. Feldmeier, *Rep. Prog. Phys.* **50**, 915 (1987).
- [4] P. Fröbrich, I.I. Gontchar, *Phys. Rep.* **292**, 131 (1998).
- [5] Y. Aritomo, T. Wada, M. Ohta, Y. Abe, *Phys. Rev.* **C59**, 796 (1999).
- [6] J. Błocki, W.J. Swiatecki, report LBL-12811 (1982).
- [7] I. Kelson, *Phys. Rev.* **B136**, 1667 (1964).
- [8] H. Krappe, J.R. Nix, A.J. Sierk, *Phys. Rev.* **C20**, 992 (1979).
- [9] W.D. Myers, W.J. Swiatecki, *Nucl. Phys.* **81**, 1 (1966).
- [10] W.D. Myers, W.J. Swiatecki, *Art. Fys.* **36**, 343 (1967).
- [11] J. Błocki, Y. Boneh, J.R. Nix, J. Randrup, M. Robel, A.J. Sierk, W.J. Swiatecki, *Ann. Phys. (NY)* **113**, 330 (1978).
- [12] J. Randrup, W.J. Swiatecki, *Nucl. Phys.* **A429**, 105 (1984).

- [13] H. Feldmeier, H. Spangenberg, *Nucl. Phys.* **A428**, 223 (1984).
- [14] J. Błocki, H. Feldmeier, W.J. Swiatecki, *Nucl. Phys.* **A459**, 145 (1986).
- [15] A. Wieloch, Z. Sosin, J. Błocki, *Acta Phys. Pol.* **B30**, 1087 (1999).
- [16] Ch. Stodel *et al.*, to be published.
- [17] O. Mazonka, C. Jarzynski, J. Błocki, *Nucl. Phys.* **A641**, 335 (1998).
- [18] O. Mazonka, J. Błocki, J. Wilczyński, *Acta Phys. Pol.* **B30**, 469 (1999).
- [19] W. Reisdorf, F.P. Hessberger, K.D. Hildenbrand, S. Hofmann, G. Münzenberg, K.H. Schmidt, W.F.W. Schneider, K. Sümmerer, G. Wirth, J.V. Kratz, K. Schlitt, C.C. Sahm, *Nucl. Phys.* **A444**, 154 (1985).